

bradscholars

Pollutant advective spreading in beach sand exposed to high-energy tides

Item Type	Article
Authors	Itugha, O.D.;Chen, D.;Guo, Yakun
Citation	Itugha OD, Chen D and Guo Y (2016) Pollutant advective spreading in beach sand exposed to high-energy tides. Estuarine, Coastal and Shelf Science. 181: 70-82.
DOI	https://doi.org/10.1016/j.ecss.2016.08.011
Rights	© 2016 Elsevier. Reproduced in accordance with the publisher's self-archiving policy. This manuscript version is made available under the CC-BY-NC-ND 4.0 license http://creativecommons.org/licenses/by-nc-nd/4.0/
Download date	2026-03-09 00:40:11
Link to Item	http://hdl.handle.net/10454/9484



The University of Bradford Institutional Repository

<http://bradscholars.brad.ac.uk>

This work is made available online in accordance with publisher policies. Please refer to the repository record for this item and our Policy Document available from the repository home page for further information.

To see the final version of this work please visit the publisher's website. Available access to the published online version may require a subscription.

Link to Publisher's version: <http://dx.doi.org/10.1016/j.ecss.2016.08.011>

Citation: Itugha OD, Chen D and Guo Y (2016) Pollutant advective spreading in beach sand exposed to high-energy tides. *Estuarine, Coastal and Shelf Science*. 181: 70-82.

Copyright statement: © 2016 Elsevier. Reproduced in accordance with the publisher's self-archiving policy. This manuscript version is made available under the CC-BY-NC-ND 4.0 license <http://creativecommons.org/licenses/by-nc-nd/4.0/>

1 Pollutant Advective Spreading in Beach Sand Exposed to High-Energy Tides

2 Okuroghoboye D. Itugha¹, Daoyi Chen² and Yakun Guo³

3 ABSTRACT

4 This paper presents field measurements in which dye solute was injected into coastal sand to
5 investigate contaminant advection in intertidal beach sand. The measurements show the
6 pathways of a contaminated plume in the unsaturated zone during both the flood and ebb tides. A
7 prescribed amount of dye tracer solution was directly injected through the topsoil, with average
8 porosity 0.3521 ± 0.01 , at predetermined locations of the River Mersey's outer estuarial beach
9 during ebb-tide. The injected dye was monitored, sampled and photographed over several tidal
10 cycles. The distinctive features of the plume (full two dimensional cross-sections), sediments and
11 water-table depth were sampled in-situ, close to the injection point (differing from previous
12 contaminant monitoring tests in aquifers). The advective movement is attributed to tidal impact
13 which is different from contaminant transport in aquifers. The experimental results show that
14 plumes have significantly large spatial variability, diverging upwards and converging
15 downwards, with a conical geometric shape which is different from the usual spherical/elliptical
16 shape reported in literature. The mean vertical motion of the plume reaches three times the top-
17 width within ten tidal cycles, exceeding the narrow bottom-width by a factor of order 2. The
18 observed transport features of the plume within the beach sand have significant relevance to
19 saltwater intrusion, surface water and groundwater quality. The field observations are unique and
20 can serve as a valuable benchmark database for relevant numerical studies.

21 **Keywords:** *Coastal foreshore, dye migration, River Mersey Estuary (RME), interstitial*
22 *hydraulics, groundwater table.*

¹Faculty of Engineering and Technology, Civil & Environmental Engineering Department, Federal University Otuoke, 400 University Boulevard, Otuoke, PMB 126, Bayelsa State, Nigeria. Email: itughaod@fuotuoke.edu.ng

²Ocean Science and Technology Division, Graduate School at Shenzhen, Tsinghua University, Shenzhen 518055, P.R. China. **Corresponding Author Email:** chen.daoyi@sz.tsinghua.edu.cn

³School of Engineering, University of Bradford, BD7 1DP, UK. Email: y.guo16@bradford.ac.uk

23 1 INTRODUCTION

24 Most contaminated beach sediments near industrial cities in Europe show relatively high
25 concentrations of heavy metals and persistent organic pollutants (POPs) even though many
26 years have passed since they were firstly polluted. This seems to be the case with estuaries
27 whose watercourses pass through urban and highly industrialised areas, even after the surface
28 water has been treated. This poses threats to the ecosystem and biodiversity due to releases
29 associated to toxic sewage, and to remediation efforts often neglecting the river bed.

30 In the United Kingdom a number of estuaries, such as the Thames, the Mersey, and the Humber,
31 have had well documented accumulation of untreated domestic and industrial sewage. One
32 special case is the River Mersey Estuary (RME, in north-west England), which is connected to
33 Liverpool Bay at the Outer Estuary (see Fig 1). It directly exchanges tidal input and output with
34 the Irish Sea through Liverpool Bay, where the sands vary from medium to fine. The catchment
35 area of the RME is densely populated and highly industrialized, and the RME is described as
36 one of the most polluted water ways in Europe with flow rates promoting high turbidities
37 (Turner et al, 2002; King et al, 2004; Jones, 2006). It has been reported that a large
38 concentration of contaminants still persists in extensive RME and Liverpool Bay intertidal
39 beach sediments. For example, concentrations of Mercury (Hg), caused by use of Castner-
40 Kellner processes, remain as high as 2 mg/kg at discharge outlets linked to chemical plants in
41 the Widnes–Runcorn areas of RME (Fox et al, 1999; Vane et al, 2007). [Mercury is associated
42 with organic matter and is toxic to marine invertebrates with potential effects on humans
43 through ingestion of fish and shellfish]. However, the toxicity levels in the sediments tend to
44 decrease in the Liverpool Bay regions away from the discharge outlets (Rogers, 2002). Burt et al
45 (1992) reported the upper and lowest mean levels of Hg in the sediments as 1.2 and 0.01 mg/kg
46 (in 40% silt), respectively. POPs, polyaromatic hydrocarbon (PAHs) and polychlorinated
47 bipheniles (PCBs), in the sediments of RME, its tributaries and Manchester Ship Canal, may
48 have originated from oil refineries, sewage, paper and chemical works, dockyards, power
49 stations and shipping activities (Jones, 2006). King et al (2004) found that PAH levels in the
50 sediments were much more concentrated at depths of 0.5-0.53m. PCB concentration in the RME
51 is believed to be higher than that in the Thames and the Humber estuaries. Recent observations
52 by Vane et al (2007) show no declining trends of PCBs but implied that the Outer Estuary areas
53 are 30 times less contaminated than the Inner Estuary. To our best knowledge, no clear
54 relationship between contaminant movement and tidally mediated fluxes in beach sediments has
55 been reported so far. However, Rogers et al (1992) suggested that the presence of these
56 substances deep in the RME sediments may have been due to tidally induced diffusive mixing.

57 Organic matter content between sandy (low organic content) and marsh sediments can also
58 strongly affect PAH concentration distribution (King et al, 2004). Huang et al (2003) identified
59 that hydrophobic organic contaminants (HOCs) can readily mix in benthic organic sediment
60 (BOS) environments. They identified the importance of understanding and quantifying varied
61 HOC properties for the prediction of transport and eventual fate in aquatic environments.

62 The vadose zone (intermediary between seawater and groundwater) of the RME intertidal beach
63 is affected by very complex hydrological processes from high-energy semidiurnal tides. The
64 beach water table rises and falls with the sea level. So water-borne sewage or sewage discharged
65 from urban, coastal recreational and industrial activities can enter and be retained or redistributed
66 (Diaw et al, 2001). Martino et al (2002) suggested that trace-metals accumulated in beach
67 sediments could be released by kinetic (advective) re-suspension processes and desorbed to the
68 overlying watercourse. Accurate field studies/measurements are limited due to the complex
69 hydrological environment as the parameters controlling convective activity in-situ become more
70 difficult to quantify (Wexler, 1992; Zhang et al, 2002; Precht and Huettel, 2004). As a result,
71 there is presently poor understanding of the movement and spreading of anthropogenic
72 substances (such as land-applied chemicals), spills and leaks that eventually enter beach
73 sediments and consequently the freshwater domain (Mao et al, 2006). This may partly explain
74 that considerably more research is conducted on contaminant transport in coastal groundwater
75 (GW) aquifers than on transport in beach sediments (Lanyon et al, 1982; Diaw et al, 2001; Mao
76 et al, 2006; Denham and Vangelas, 2008). More studies on groundwater behavior in sandy
77 beaches, with relationships between tide and water-table, can be found in Baird and Horn
78 (1996); Turner and Leatherman (1997); Kalbus et al (2006); and Berkowitz et al (2008).

79 Pressure fluctuations can have a significant impact on interstitial oxygenation processes, thus on
80 fates of contaminants and in some cases on aquatic life (McLachlan, 1989; Precht and Huettel,
81 2004). Water movement is routed via complex pores and varies with depth and degree of
82 compaction. The properties of the sand (porosity ϕ , grain size and grading) and the dye (density
83 ρ , and dynamic viscosity μ) are therefore important to determine the role of hydraulic
84 conductivity (Fetter 1999). This is because the local unsaturated hydraulic conductivity depends
85 on the degree of soil - water content and/or pressure head (Mohanty et al. 1994; Gupta et al.
86 1993). Typical porosity for medium to fine sand ranges from 26% to 53% (Domenico and
87 Schwartz, 1997). Barnes (1995) estimated the hydraulic conductivity values of sand and sand-
88 gravel mixtures to vary significantly from 0.036m/hr to 36m/hr respectively. Fox et al (1999)
89 showed that the sediment cores of the RME (e.g., Widnes – Runcorn areas) are made up of 2-5%
90 sand with size distribution of 63-2000 μ m, 70-75% silt (2-63 μ m), and 25-27% clay (<2 μ m).

91 The use of conservative tracers to simulate contaminant movement in the field is a known robust
92 technique. However, Robbins (1989), Callaghan and Codd (1998) and Precht and Huettel (2004)
93 have shown that use of tracer monitoring devices in intertidal beach sand may not provide
94 reliable qualitative and quantitative concentration data. This is because the intrusive techniques,
95 such as probes and positron emission tomography, can affect the natural flow regime in the
96 subsurface environment.

97 This study was motivated to attract attention of remediation efforts to consider flushing of the
98 river bed sediments and foreshore (water quality management issues), along with treatment of
99 the surface water in estuarine areas of this nature. It reveals that tides can induce surface water –
100 vadose zone - groundwater interactive transport. The study was also motivated by the fact that
101 most methods for monitoring the contaminant in the field involved intrusive techniques, such as
102 probes and positron emission tomography, which are known to affect the natural flow regime in
103 the subsurface environment, hence may not present the expected natural phenomenon. Therefore,
104 there is a need to visualize full shapes of the plume in the field in order to investigate the
105 contaminant movement in beach.

106 2 SITE CONDITION AND METHODOLOGY

107 A non-intrusive method is employed is employed to investigate the contaminant movement in
108 beach sand subject to large tidal range in this study. A conservative tracer (dye) is injected
109 0.05m below the unsaturated beach sediment surface. The experiments lasted over one to ten
110 semidiurnal tidal cycles during the summer months of 2006 and 2007. Sediment characteristics,
111 water table depth of the intertidal zone and the spatial variability of fully extracted plumes were
112 sampled, processed and analyzed.

113 2.1 Study area

114 The experiments were carried out in Liverpool Bay (the RME Outer Estuary injection site
115 (OEIS) and Narrows (Narrows Estuary injection site (NEIS); 53'26"N and 03'02"W) at New
116 Brighton, England (see Fig 1). The Mersey Estuary of Northwest England has an area of
117 approximately 5000 km², with a history as one of the most polluted estuaries in Europe (WPRL,
118 1974; Jones, 2000; Vane et al, 2007). Its catchment has a high density of population up to 5
119 million, including the major municipalities of Liverpool and Manchester, and was heavily
120 industrialized. RME consists of four divisions, namely the Upper, the Inner, the Narrows and
121 the Outer Estuary.

122 The Outer Estuary includes a large intertidal sand beach, with a range of facilities at the
123 sheltered corner of the coast and a marine lake seawards of the shoreline. The Narrows is an
124 ostrich-neck-like convergence with breadth measuring 1.0-1.5 km and a maximum depth of 30
125 m. The broader Inner Estuary is a characteristic mixed estuary with salinity measuring an
126 equivalent of 4g/l at low tides to 11g/l at high tides. The current passing through the Narrows has
127 a velocity up to 2m/s at spring tides.

128 Generally speaking, tides from the Irish Sea directly enter the RME during the flood phase
129 through Liverpool Bay and discharge to the Irish Sea during the ebb phase. Tidal range is
130 between 10.7m (maximum springs) and 4.0m (minimum neaps). The water volume of the RME
131 varies from $0.7 \times 10^7 \text{ m}^3$ at low tide to $3.5 \times 10^8 \text{ m}^3$ at high tide, indicating a significant effect on
132 the catchment. The mean sea level (MSL) is about 5.214m above the ordinance datum (AOD)
133 (Admiralty Tide Tables, 2005). The strong tidal currents sustain large sandbank build-up in the
134 estuary. The sheltered boundary may be affected through groundwater flow from the wave run-
135 up and infiltration at the intertidal reach.

136 The exposed beach consists of a variation of medium to fine sand and localized mud banks. The
137 aquifers of sheltered and of intertidal boundaries receive water from the prevailing tidal regime.
138 There are several borehole wells that litter the sheltered boundary, the closest of which to any of
139 the injection sites is about 1km. The Marine Lake however is less than 20.0m from OEIS-IZ (A)
140 and has depth varying from 5.0m at the west end to about 0.5m at the east end. The intertidal
141 zone of OEIS from the inland beach bank to the shoreline at low ebbs averages between 345m
142 and 450m. At the NEIS area, the width of the intertidal zone varies from about 45m to 368m.

143 2.2 Experimental design, material and method

144 2.2.1 Site preparation, tracer type and dye injection

145 Tests were carried out at three OEIS injection zones (IZs), namely A, B, and C, and two NEIS
146 injection zones, namely A and B. The activities on site included surveillance and delineation of
147 the site, dye injection, sampling, plume measurement, core sample collection, GPS location and
148 elevation recording. Each IZ defines multiple sampling points (SPs, see Table 1 which lists the
149 total injected points and the sampled injected points.) with two rectangular dimensions of 1.5 x
150 2.5 m^2 and $2.5 \times 2.5 \text{ m}^2$ on the unsaturated beach surface. Dye injection was not repeated on any
151 previously used SP to avoid the effect associated with disturbed flow field resulted from
152 previous injection and sampling activities. The SPs were not equally spaced apart but separated
153 by a distance of at least 5.0m as measured by a 15.0m fiberglass tape. The rectangular arrays
154 were divided into 0.5 (length, l) x 0.5 (breadth, b) m^2 square cells so that each SP consists of 15

155 or 25 injection points (IPs) in 3x5 or 5x5 column/row grids (arrays) respectively (see Fig 2 and
156 Table 1). This means that the injected dye was entrapped within a volume of 0.13125 m^3 ($l=0.5$)
157 \times ($b=0.5$) \times (depth $h=0.525$). The locations of SPs were recorded using a 12-channel Garmin
158 GPS 76 marine navigator with precision of about $\pm 2\text{m}$. The inject dye was a red color 810
159 (E124) conservative agent with 4.3% pure dye content, and density of $0.947\text{g}/\text{cm}^3 - 1.022\text{g}/\text{cm}^3$.
160 Since the solution is conservative food dye, it is expected that it is not absorbed to the sand
161 surface.

162 2.2.2 Tracer solution injection and monitoring

163 The dye solution (5.0ml portion) was injected at 0.05m below the beach surface (about 1.55m
164 below the high tide mark) during low water. The choice of 0.05 m injection depth is considered
165 to be reasonable since the first 0.05m coastal sand region readily stimulates oxygen injection and
166 utilization into deeper layers (Rusch et al 2000; Ehrenhauss and Huettel 2004). A 10.0ml
167 Pressure-Lok precision sampling purge and trap syringe system with appropriately calibrated
168 hypodermic needles of size 0.028" x 0.012" x 2" was used to inject the dye. Fig 3 demonstrates
169 that the sampling zone (area) at OEIS-IZ(A & B) generally varies between about 75 to 185m
170 offshore from the inland beach back barriers. The vertical line of injection (needle-line) is as thin
171 as the natural soil pores hence assumed non-intrusive. The amount of solution injected and the
172 depth of injection remained the same in the experiments. Field activities were repeated through
173 three months during the summer (17/April-17/July 2006; 2007), always at neap tides. Though
174 winter tests were carried out for three months (22/November 2005-19/January 2006) at OEIS-
175 IZ(A), the success rate was low due to harsh field conditions. The atmospheric environment
176 during the experiments was not only under sub-zero temperatures but also very windy during
177 November 2005 to January 2006. As such, it was not convenient (health/safety and clarity-wise)
178 to conduct sampling/measurement/recording activities in the field, meanwhile to ensure the
179 measurement accuracy. Therefore, only the summer samples at OEIS-IZ (A and B) are reported
180 here. The injected sample was monitored through several tidal cycles (1/4, 1, 2, 4, 6, 8, 10, 12,
181 and 14). The injection always took place at the start of the low tide, therefore, there is no
182 difference of start state of tide and the state of tide effect on the spread of dye is the same.

183 2.2.3 Tracer plume sampling, measurement and parameterization

184 On detecting the contaminated surface area ($l \times b$), each boundary was carefully sectioned using
185 hand trowels to penetrate the undisturbed plume domain. The volume ($l \times b \times h$) of the sand from
186 the surface was sliced from the edge towards the center of the square ($l \times b$). This was done on
187 each occasion to maximize recovery and measurement of the full 2D plume shape (see Fig 4).

188 The geometry of the plume was measured from the photograph taken using a Nikon Coolpix
189 8800 digital camera of 8.0 effective megapixels. Figures 4a, b and c are the photos taken at
190 various times indicated in figure caption after injection. It shows the vertical extent of plume,
191 depth of plume center and the top and bottom widths of plume at various elapse times of
192 injection. Figure 5 demonstrates and summarizes these parameters. A Cartesian coordinate
193 system is established using the horizontal line passing the injection point as the x-axis and a
194 vertical line some distance away from the plume center line as the y-axis.

195 As the vertical advective spreading is a cone shape, a trapezoidal shape is adopted (see Fig 5) to
196 evaluate the plume. The top and bottom (front) width of the plume are defined as W_1 and W_2
197 respectively. The infiltration depth is the vadose zone with horizontally infinite dimensions. The
198 depth GI is the depth of injection at $I = (0.25, -0.05)$ while GH represents Y_0 , the depth of the
199 center of mass of the cone (Fig 5; Y is the (vertical) depth coordinate).

200 2.2.4 Depth-to-water and water-table elevation measurement

201 Water table elevation (WTE) at OEIS-IZ (A and B) and NEIS-IZ (A) was determined by
202 measuring the depth-to-water table (DTW) and beach surface elevation using a GPSMAP 62S
203 which has 5ft – 12ft margin of error. DTW was taken as the depth below the beach surface to
204 the top of the saturated material (subtidal), where the mean pore pressure is atmospheric (zero)
205 (Nielsen, 1997). The elevation and shape of the water table surface respond to surface water
206 features resulting from recharge and discharge changes. The DTW measurements averaged to
207 about 0.525m, which is relevant towards the depth of IP in relation to the high tide mark (HTM,
208 see Fig 3). Fig 6 is a typical example showing the variations of the mean elevations of the
209 beach surface and the depth to water table with beach width. The water-level data were
210 converted from depth below surface to WTE using the beach surface elevation (BSE) measured
211 by GPS. In Fig 7, the Kozeny-Carman relation (Klute and Dirksen, 1986) is applied to show the
212 permeability of core samples taken from injection sites with different grain-sizes. Fig. 8 shows
213 the influence of tidal variation on the water level of the closest borehole well to the OEIS-IZ and
214 NEIS-IZ, and marine lake water levels at the sheltered coast.

215 3 RESULTS AND DISCUSSIONS

216 3.1 Physical properties of beach sediment

217 The grain-size distribution of the cores (Samples A-F) showed 96.3 to 100% sand (medium to
218 fines), 1.3-3.4% silt, 0.1-0.3% clay and 1.4-3.7% mud. The median grain size (d_{50}) is spatially
219 variable ranging between 0.196m and 0.259m, while the geometric mean of lognormal

220 distribution of the diameter varied from 0.176mm to 0.258mm. The effective grain-size (d_{10})
221 also varied between 0.121mm and 0.188mm. The ratio of geometric mean grain size to median
222 grain-size varied from 0.901 to 0.996, with particle standard deviation varying between 1.266
223 and 1.966. The porosity of the sand determined in the laboratory using the volume of voids to
224 total volume was 0.352 with confidence level of ± 0.01 . The coefficient of uniformity C_u was
225 1.531 ± 0.08 (95% confidence intervals) < 4 . The coefficient of curvature C_c , which is dependent
226 on factors of shape and symmetry, was 0.287 ± 0.01 (95% confidence intervals). Values of C_u
227 between 1 and 3 normally define well-graded sediment materials. The value of C_u here shows
228 that size is reasonably regular, hence high porosity and vulnerability.

229 The optimal moisture content in the capillary fringe above the water table at the maximum
230 density of 1309.4 kg/m^3 was determined as 20.5% using the first 15cm of unsaturated core
231 samples from OEIS. The specific yield varied between 0.176 ± 0.004 and 0.214 ± 0.02 using the
232 untreated core specimens. Averaged permeability K of the sampled sand at OEIS-IZ (A & B)
233 and NEIS-IZ(A) was determined to be $1.482 \times 10^{-5} \text{ m/s}$ using the method of the Falling-head
234 (Klute and Dirksen, 1986).

235 Fig 7 is the comparison of permeability of the cores for the sites using the Kozeny-Carman
236 relation, which is adopted because it incorporates grain-size distribution and shape (Carrier
237 2003). Fig 7 shows that the permeability of the investigated intertidal sediments decreases with
238 the increasing of the sand percentage passing the sieve size. Larger difference of the
239 permeability of sediments at various sites is found for the lower sand percentage passing the
240 sieve size while this difference decreases for higher sand percentage of passing the sieve size.
241 More pressure is needed to squeeze the injectate through sediment with low permeability (i.e.
242 high sand percent passing) than in zones with high permeability (i.e., low sand percent passing).
243 The grain-size distribution of the cores in this study showing high sand percent passing is mainly
244 from medium to fine sand. It is also seen that the permeability of the intertidal sediments at the
245 OEIS-IZ (A) was much higher than that of others at the lower sand percentage passing the sieve
246 size. However, the permeability of sand at the OEIS-IZ (A) decreases sharply with the increasing
247 of sand percentage passing the sieve size and is lower than that of sediments taken in other sites.
248 The results are in good agreement with published data in literature for the same category of
249 marine sand (Todd, 1980; Mason, 1997; Li et al, 2009). In-situ values of permeability are usually
250 larger than laboratory estimates as shown in Li et al (2009), so the values of K found in this
251 study are at the lower end.

252 3.2 Influence on local groundwater (GW) table by tidal events

253 Monthly-averaged Liverpool sea level from the records at the British Oceanographic Data Centre
254 (BODC) was 5.154m in August 1991 and rose to 5.177m in December 2006 while the annual
255 mean of 1991 was 5.158m and by 2006 it was 5.401m. Woodworth et al (1999) showed in an
256 earlier study of data covering the period of 1858 to 1998 from all three (3) tidal water stage
257 markers (Gladstone, Alfred, and Princes Pier) that the mean sea levels had a relative increase of
258 0.17m. The tides at Liverpool are predominantly semi-diurnal with mean tidal range of 6.7m
259 (Woodworth, P. L. and Blackman, D. L. (2002)). The maximum high water and the minimum
260 low water sea levels observed during this period were recorded as 10.821m and -0.181m on
261 10/02/1997 at 1244hrs and 20/02/1996 at 1915hrs respectively. Fig 8 shows the effect of the
262 change of water head at the seaward boundary on the coastal barrier aquifers in 2006. The rise
263 and fall in the data shows that the local groundwater system may be connected or influenced by
264 tidal events.

265 The marine lake water levels were averaged between 2006 and 2007 for different (west to east)
266 locations. The highest water level in the lake was recorded at the western end.

267 3.3 Depth of advection and spreading scenario of contaminant in beach sand

268 To investigate the advection and spreading of plumes, dimensions averaged for the sites in Fig 5
269 will be used to plot the movement of plumes in space with time.

270 3.3.1 Scenario at OEIS-IZ (A) – summer

271 A ‘no-flood’ case was initially tested by injecting the conservative dye through the unsaturated
272 beach surface and waiting for about 5 hours. The well water level variations were taken from a
273 relatively distant borehole-well (sj39/130). A second test was an extension to one complete tidal
274 cycle where dye was injected while the beach surface was unsaturated and then waiting through
275 one full saturation-unsaturation cycle. About 50 samples were collected at different locations and
276 Fig 4a, b and c shows the comparison of the output from some of the tests. In Fig 4a, the dye was
277 allowed for up to 5 hours in the sediments with no tidal flooding on the beach. All the plume
278 pools in this case look identically circular or spherical in shape when sampled. The mean cross-
279 sectional area was within a 95% confidence interval of $3.384 \times 10^{-3} \pm 2.6 \times 10^{-4} \text{m}^2$. This type of
280 response was attributed to convective flow since there was no visible recharge that initiated the
281 spread. Again, when the dye was monitored through one complete tidal (saturation-unsaturation)
282 cycle, the plume pools changed to conical shapes covering an averaged area of about
283 $0.0032 \pm 0.001 \text{m}^2$ within the entrapment volume ($l \times b \times h$). A further change evolved in the
284 conical contour when the monitoring period was increased to two complete tidal cycles (Fig 4c).

285 The area of these plumes was a similar order of magnitude as in the one-cycle case. Without
286 field observations, intuition for plumes in a porous medium would suggest either a spherical or
287 elliptical shape. Conical shapes of this nature have not been reported in literature, at least not to
288 the authors' knowledge. The determination of the magnitude of the plume and shape could help
289 towards understanding the extent of dye concentration, direction of distribution and eventual fate
290 in intertidal coastal zones with similar properties. The formation of plumes as shown in Figs 9
291 (Top and Bottom) demonstrates the effect of pressure variation in the vadose zone. It is seen
292 from Figs 9 (Top and Bottom) that the inclination of the tidally induced plumes highlights the
293 processes of horizontal mass transport and pressure gradient variation controlling coastal
294 groundwater table fluctuation. Fig 9 (Top) shows a collection of samples representing the
295 general behavior of the injective in OEIS-IZ (A) from day-1 to day-5. It shows the progressive
296 formation of a plume by advective spreading in space with time. With infiltration, the pressure in
297 the pore medium decreases as zones of low pressure is created in the area of the IP. The
298 progression of subsidence affecting the plume in space with time can be observed clearly. The
299 H_p (height of plume-top below injection-position) varies from 0.09m (about 1.59m below HTM)
300 on day 1 to 0.19 (about 1.69m below HTM) by day 5. The visual profile shows that the plume
301 enters the water table by about day 5 in this particular case. This may be caused by the
302 infiltration from the flood tide which drives the plume down from the initial position (high
303 conductivity zone) to a low conductivity region. The damping effects on the plume (difference in
304 the movement of the plume at the high conductivity zone and at the low conductivity zone) at the
305 top of the sediments would be therefore small in this case compared to greater depths. This
306 characteristic behavior can be attributed to the mechanism of mass flux in the direction of the
307 low conductivity region due to the net horizontal tidal flow, which induces level changes in the
308 water table. As the shoreline moves inland and offshore with tidal level oscillations, the plume
309 adapts to the pressure alteration above the capillary fringe in the unsaturated flow. Assuming the
310 pressure at the beach face be constant, the temporal variations of the pressure gradient in the
311 capillary fringe will mean that the zero-pressure location changes instantaneously. The pressure-
312 gradient-induced water-table fluctuation is therefore responsible for the rate of advective spread
313 of the injected dye in space. The orderly transformation of the plume describing the direction of
314 mass transfer can thus be associated to the effect of fluctuations within the capillary zone. At
315 varying levels of the instantaneous zero-pressure location during recharge, the capillary fringe
316 approaches uniformity such that the local mass transfer (plume movement) rate is controlled by
317 the low permeable materials with hardly visible water movement. In this particular scenario, the
318 effect of the capillary fringe on mass transport may be small at the surficial region of the beach
319 due to the high permeability. Also, the beach surface may experience low-frequency sea level

320 oscillations with a corresponding response from the water table. However at greater depths (from
321 about 1.5m below HTM), the effects of the capillary fringe become significant with low
322 permeability as high-frequency sea level oscillations (tides) take over. This makes the plume
323 front (bottom width) to spread less and become narrower (see Fig 9 (Top)). The effect of a
324 receding tide on the injectate could be more significant than recharge, due to the slow expulsion
325 of capillary water. Observations by Boufadel et al (2006) showed that tidal floods pushed the
326 tracer mass vertically downwards along mean flow gradients while ebb-tides influenced
327 spreading with the sea level oscillatory motion. The features in the frames (Fig 9 (Top))
328 demonstrate subsidence, movement and potential access of the contaminant into groundwater.

329 3.3.2 Scenario at OEIS-IZ (B) – summer

330 To give an objective interpretation of the complex scenarios here, the cases OEIS-IZ (B) were
331 split into OEIS-IZ (B(i)) with subsidence similar to that observed in OEIS-IZ (A) and OEIS-IZ
332 (B(ii)) lacking much subsidence. However, in OEIS-IZ (B(i)) cases the rate of subsidence and
333 vertical spreading tends to decrease with depth, limiting the movement of the center of mass. In
334 the case of OEIS-IZ (B(ii)), the resulting plume simultaneously diverges upwards and converges
335 downwards. The results are unique and show that the surficial region of the sediments is prone
336 to rapid rates of matter exchange, readily stimulating oxygen injection and utilization into
337 deeper layers (Ehrenhauss and Huettel, 2004) as shown in Figs 9 (Top and Bottom). In Fig 9
338 (Bottom) the H_p relapses to 0.01m (about 1.51m below HTM) or 0.06m below surface after two
339 complete tidal cycles (day 1). The plume further spreads upward to the surface water-sediment
340 interface where the pressure is about constant, showing potential loss of contaminant to surface
341 water from day 2 to day 5. The results show that the water tables at these two locations, namely
342 OEIS-IZ (B(i)) and OEIS-IZ (B(ii)), are affected by the same tidal conditions but the plumes
343 respond differently. Clearly the tidal oscillations and pressure fluctuations on the beach-sand
344 are not uniform, hence the varying level of plume response. However, the pattern of spread
345 (conically shaped plume) conforms to the inland-offshore oscillatory direction of net horizontal
346 water movement.

347 This means that the effect of tides on the trapped contaminant (injectate) could also depend on
348 the level and frequency of instantaneous water table fluctuation. The observation of the plume
349 response in this area shows that the effects of sediment permeability and capillary pressure
350 change are significant. Therefore, the effect of tidal water-level-induced BWT fluctuations on
351 the trapped contaminant will depend on the permeability, magnitude and frequency of tidal
352 oscillation over the beach. Furthermore, in addition to permeability, the topography of the beach

353 face could influence the frequency of water table fluctuation in contrast to water movement in
354 the subsurface. This observed behavior differing between OEIS-IZ (A) and OEIS-IZ (B) can be
355 ascribed to the gravity development (Beinhorn et al, 2005) since the topography of the foreshore
356 is not uniform. The plume widths shown in Fig 12 have potential implications for management
357 decisions with respect to the surface and groundwater quality.

358 3.4 Analysis of spatial variability of plume

359 Fig 10 shows the average of plumes from Site-1 and Site-A of OEIS-IZ (A) which effectively
360 relate to the movement described in Section 3.3. In other words, the response is such that as the
361 low-frequency tide pushes the shoreline boundary inland, the high-frequency water table
362 fluctuates. The movement of these two phases should therefore be responsible for the mass
363 movement and capillary pressure effects (Li et al., 1997). For example, during the formation
364 process (advective spreading of the plume), by the 2nd complete tidal-cycle the plume moves
365 such that the center of mass moves down from the injection point (0.25,-0.05) to H (0.25,-0.169).
366 After the 6th and 10th cycles the center moves further to I (0.25,-0.223) and N (0.25,-0.286)
367 respectively while maintaining the full 2D-conical profile. This observation is consistent with
368 Fig 10 where the first two tidal cycles also differ from the 10th. The center moves through point I
369 (0.25,-0.1427) after 4 cycles to D₁ (0.25,-0.3375) after 10 cycles (all in meters). The negative
370 sign indicates that the dye is below the beach sediment surface. The depths are subject to
371 adjustment with respect to the HTM (about 1.50m above the beach surface at the injection
372 region). Also from the samples averaged in OEIS-IZ (B), two distinct responses belonging to
373 sites B(i) and B(ii) are observed. In site B(i), it was found that the full plume subsides (shifted
374 downwards) like the previous case, but the fall-rate of the center of mass from the IP diminishes
375 with increasing time . In site B(ii) [Fig 11] however, the plumes advect and spread while
376 diverging upwards and converging downwards simultaneously. These characteristic observations
377 could not have been driven by a singular environmental factor but by a combination of processes
378 (tidal and water table fluctuations inducing pressure gradients on the foreshore, pore-fluid
379 salinity, sediment properties). The combination here is unique and has not been reported in
380 literature. For instance, the dye plumes reveal persistent vertical conical gradients, not
381 spherical/elliptical shapes. It demonstrates unique and different transport of dye plume
382 (pollutant) in tidal beach from transport in aquifers. The tidal impact on pollutant movement is
383 different from contaminant transport in aquifers. The effect of each of these processes (tidal and
384 water table fluctuations, etc. as above) on these observations could be further explored. The
385 slowing translation of the center of mass in Fig 11 could be attributed to vertical mixing limiting
386 kinetic energy due to interception from re-suspension flows. Moreover, since the beach acts as a

387 filtrate and burial post, early minute deposits could consolidate deeper for new arrivals to
388 continue the building process, hence, permeability differences could appear at the sample area.
389 Furthermore, great average vertical cross-section of the plume is found in Fig 11, giving the
390 impression of increased flow or mixing rates at the sediment grain-water interfaces at sites B.
391 This could be due to the near-surface position of the center of mass, which is prone to rapid rates
392 of matter exchange at the interface (Ehrenhauss and Huettel, 2004), since there is less or no
393 evidence of subsidence at sites B.

394 The observations from Figs 10 - 11 clearly show that the dye plume varies strongly with time.
395 The averaged plume patterns shown in Figs 10-11 also vary with location as described in the
396 qualitative examples (see Fig 9). This implies that the tidal oscillations and pressure fluctuations
397 on the beach-sand are also not uniform, and cause wider plume variability in space.

398 3.4.1 Analytic discussion of the advective spreading of plume features

399 Figs 12-13 demonstrate that the features of the plume vary considerably at each site but with a
400 general tendency to spread. Fig 12 shows a description of mean data points of the bottom width
401 W_2 for site 1, site A and site B. On average W_2 narrows spatially to between about 0.03 and
402 0.06m within the duration of the experiments in these beach sediments. The narrowing of W_2 is
403 not sustained in space and time as shown in the distribution of data points. The similar concave
404 trend in the curves suggests similarity of the beach characteristic properties. As the plume front
405 penetrates deeper, the trend of spreading becomes highly variable, and dampens between the
406 third and fourth days as suggested in the upward concave curves. The narrowing implies that
407 permeability of these beach sediments decreases with depth. Also, in Fig 12, the Top width W_1
408 diverges with mean length varying between 0.06 and 0.11m. The larger values are associated
409 with greater permeability and near-surface net horizontal water movement. Tidal oscillation
410 causes the water table elevation to change or fluctuate instantaneously, which tends to enhance
411 the mixing rates within the top sediment-water interface layer. The damping effect will be
412 therefore limited by the high permeability of the surficial sediments as the shoreline water
413 propagates inland or offshore. The contraction in the curves as downward concave in sites B(i)
414 & B(ii) may not necessarily mean decreasing mixing rates at the near-surface but rather
415 reduction in opaqueness of the dye due to loss. The observations clearly show higher horizontal
416 mixing rates at the near-surface than that at greater depths, as shown in Fig 12. Fig 13 (a) shows
417 the average depth of the top of the plume below the surface of the sediment (about 1.5m below
418 HTM) at the sites under investigation. It is seen from Fig 13 (a) that the general trend of the
419 averaged depth-to-surface data is related to a steady subsidence with time. The variations are

420 consistent between all the sites with the exception of B(ii) which is associated with the examples
421 of upward divergence observed in Fig 9. Shum (1995) acknowledged that the net horizontal
422 wave driven oscillatory water movement induces sufficient fluxes over the ripple sand beach bed
423 to initiate interfacial hydraulic flow. It can be seen here that at later times the top of the plume
424 moved towards the near-surface sediment-water interface. This is an example of loss to surface
425 water from buried point-sources as shown in Fig 9. The statistical averaged data from the sites
426 shown in Fig 13(b) reveal that the vertical length of the plume varies between about 0.12 and
427 0.35m in space with time. The nonlinearity in the curves shows that the spreading slows and is
428 even reversed at some later times. This is expressed in the downward-concave curves; from
429 about day 3 or 4 the plumes tend to contract. This is caused by the vertical mixing limiting
430 kinetic energy due to low permeability at more consolidated depths. However, plumes lengthen
431 fast at sites B(ii) compared to the rest of sites. This may be due to continual upward and
432 downward movement in response to the boundary condition changes at the beach face and
433 sediment-water table interface. It is estimated that the mean depth of this segregated pore region
434 is about $Y = 1.724\text{m}$ below the HTM. Fig 13 (c) shows the averaged location of center of mass
435 (Y_0) for sites 1, A & B. From the averaged analysis in Figs 10-11, Y_0 increases from 0.14 to
436 0.34m (about 1.64 – 1.84m below the HTM) at OIES-IZ(A), from 0.13 to 0.29m at B(i) and 0.11
437 to 0.18m at B(ii). These values of Y_0 reflect the different patterns of contaminant mass transport
438 observed at the two sites. This includes the fact that there is relative lack of subsidence in OIES-
439 IZ (B(ii)). The observations are complex but the underlying interpretation may not deviate
440 extensively from the basic understanding of induced internal waves or pressure variation
441 generated through the rough permeable subsurface. In Fig 13 (d) the line represents the
442 coefficient of variation (0.045 m/day) with time of the location of the center of mass Y_0 averaged
443 from all the sites. The coefficient of variation shows that after injection the centre of the plume
444 moves down from about 0.09m to 0.315m (about 1.6m – 1.82m below the HTM) by the end of
445 the fifth day. Increased uncertainty in the centre of mass location with time could influence the
446 quantification of the contaminant distribution. However, the center-line (linear model) is a good
447 statistical indicator of the outcome.

448 The observations in this field study mostly agree with the findings from related studies. For
449 instance, Horn (2002) showed that tidal current modulation and water table pumping were
450 characteristic factors affecting contaminants in beach sediments exposed to strong tides. While
451 these factors distribute tidal energy through relatively large space, they are also able to cause the
452 migration of dye in the beach subsurface. Boufadel et al (2006) observed that flood-tides draw
453 the tracer mass down vertically along mean flow gradients whereas ebb-tides influence them to

454 spread in-tune with the oscillatory motions. The divergence and convergence of W_1 and W_2
455 respectively are in agreement with observations in literature. Webster (1992) and Williams et al
456 (2003) concluded in their observations that advective dispersion may control transport at the
457 surficial pore regions of sediments while shear dispersion dominates at deeper levels due to
458 sustained tidal and wave currents. It is expected that more of the dye will be lost to surface
459 water at OEIS-IZ (B) than at OEIS-IZ (A) where the tracer predominantly moved downwards
460 and may subsequently enter the groundwater aquifer. Reimers et al (2004) found the mean
461 downward flow to decrease downwards.

462 4 UNCERTAINTY CHARACTERISATION

463 The spatial variability of the dye was monitored over time and sampled to investigate the
464 transformation at the source. The resulting plume was then manually measured in the field.
465 Errors in this quantification process could result in uncertainties due to several factors. For
466 example, it was not possible to visualize and measure instantaneously, the variables determining
467 the transitional stages and differences in the behaviour of the dye at the OEIS-IZ (A) and OEIS-
468 IZ (B). The potential sources of uncertainty in this case therefore may be greater than in surface-
469 water transport experiments. However, our method enables direct visualization of the
470 advectively-spreading plume associated with the movement of the dye in the subsurface. Three
471 sources of uncertainty that could be associated with the data quantification process therefore
472 could be: (1) uncertainty in data collection due to measurement error and bias; (2) variability of
473 measured parameters, arising from the investigators' view and method of assessment of
474 'opaqueness' of the spread plume; and (3) measurement errors leading to uncertainty of
475 parameter estimation, such as incomplete sampling (e.g., limited knowledge of the beach sand
476 properties) and uncertain boundary conditions.

477 The aforementioned uncertainty sources in this study therefore could be attributed to high
478 variability of soil compaction and pore-size distribution. Additionally, the events monitored
479 occurred under periodic interchanges between saturated and unsaturated beach material
480 (intertidal). This implies that the hydraulic conductivity will also vary with position within the
481 subsurface granular regions. Soil-water tension or moisture content when unsaturated is
482 important information for uncertainty reduction in dye displacement. The measurement of the
483 travel path described in our conical plume formation therefore is informative and an important
484 factor towards reducing uncertainty of displacement rates in coastal subsurface materials.

485 5 SUMMARY AND CONCLUSION

486 We investigate the spatial variability of contaminants in a coastal intertidal sand beach using

487 results from field experiments. The experiments involve injection of tracer dye into the top soil
488 at five different sites, and geotechnical study. After the completion of each session of injection,
489 the spatial variability of the evolving plume in the field is monitored over time, sampled at the
490 source and manually measured. The process is repeated up to seven consecutive days over a
491 period of four summer months in two years and the transport of the tracer plume analyzed to
492 quantify the injectate advective distribution. The procedure centres on the beach-sand vadose
493 zone of the coastal foreshore in contrast to contaminant transport in groundwater aquifer studies.
494 In addition, the method differs from previous studies where the injection position of the dye
495 (source point) was different from the monitoring point.

496 The evolved range of dye plumes found here has not been reported in literature. Based on the
497 features analyzed, the plumes show persistent vertical conical gradients instead of the widely
498 known spherical/elliptical shapes. The features analyzed can be utilized to evaluate flow rates
499 (pore velocity), dispersion, and concentration data with a view to determine groundwater flow
500 paths and contaminants' fates in intertidal coastal beach sediments. The visual accounts of the
501 temporal and spatial variations of the plume are presented with satisfactory evidence of the
502 response mechanism in the subsurface. The vertical profiles of plume cross-section can be
503 related to local influence of flow ponding and low hydraulic conductivity zones with localized
504 and dense accumulation stages. The sampled temporal and spatial plume data are insightful, and
505 can inform relevant future numerical studies and practice-based research.

506 Results from this field study at the RME suggest that dye discharges into watercourses can
507 actually enter coastal beach sediments through diffusive fluxes due to tides. The fluxes
508 according to the study can also drive beach-sediment-applied-dye to resurface in seawater
509 courses and also enter groundwater courses. A recent example is the 2010 widely publicized
510 Gulf of Mexico oil accident where crude oil was found deep in beach sediment. Similar
511 scenarios have also been reported in the crude-oil-rich Niger Delta regions of Nigeria where oil
512 leaks due to rupture from submerged pipelines enter surface and groundwater courses, causing
513 serious catchment concerns. This is also in agreement with findings by Boudreau et al (2001)
514 and Boufadel et al (2006) that the surficial inland - offshore tides can induce large fluxes
515 exceeding interstitial diffusive flux in the beach vadose zone. The ability therefore to visualize
516 naturally induced advective transport of contaminant dye at the sediment-water interface can be
517 a robust means of assessing fate through groundwater tracing techniques.

518 It is expected that this study will provide the unique benchmark dataset for numerical modelers
519 to validate their models, which in turn could be used to extend the current field study in terms of
520 including broad ranges of key parameters.

521

522 **Acknowledgement:** The research reported in this paper is financially supported by China
523 Ministry of Science and Technology 973 program (2014CB745001), Special Program of future
524 development in Shenzhen (201411201645511650) and Shenzhen Key Laboratory for Coastal
525 Ocean Dynamic and Environment (ZDSY20130402163735964). The constructive comments
526 and suggestions made by the Associate Editor and four anonymous Reviewers have greatly
527 improved and enhanced the quality of the paper.

528

529 REFERENCES

- 530 Admiralty (2005). *Admiralty Tide Tables*. Volume 1, 2006. Admiralty Charts and Publications,
531 Chart NP201. United Kingdom Hydrographic Office, Taunton.
- 532 Arch, J. Stephenson, E. and Maltman, A. (1993). Factors Affecting the Containment Properties
533 of Natural Clays, Proc. Conf. the Engineering Geology of Waste Disposal and Storage, Cardiff,
534 pp 263-272.
- 535 Ataie-Ashtiani, B., Volker, R. E. and Lockington, D. A. (2001). Tidal effects on groundwater
536 dynamics in unconfined aquifers. *Hydrological Processes*, **15**, 655–669.
- 537 Ataie-Ashtiani, B., Volker, R.E., Lockington, D.A., (1999). Tidal effects on sea water intrusion
538 in un- confined aquifers. *Journal of Hydrology* 216, 17-31.
- 539 Baird, A. J., Horn, D. P. 1996. Monitoring and modelling groundwater behaviour in sandy
540 beaches. *Journal of Coastal Research* 12(3): 630–640.
- 541 Banin, A. and D.M. Anderson (1974) Effects of salt concentration changes during freezing on
542 the unfrozen water content of porous materials. *Water Resources Research*, 10: 124–128.
- 543 Beinhorn, M., Dietrich, P., Kolditz, O. 2005. 3-D numerical evaluation of density effects on
544 tracer tests. *Journal of Contaminant Hydrology* 81(1-4): 89-105.
- 545 Berkowitz, B., Dror, I., Yaron, B. 2008. Contaminant Geochemistry: Interactions and
546 Transport in the Subsurface Environment. Springer-Verlag Berlin Heidelberg.
- 547 Blott, S. J. and Pye, K. (2001). Gradistat: A grain size distribution and statistics package for the
548 analysis of unconsolidated sediments. *Earth Surface Processes and Landforms* **26**, 1237–1248.
- 549 Boufadel, M. C., Suidan, M. T. and Venosa, A. D. (2006) Tracer Studies in Laboratory Beach
550 Simulating Tidal Influences. *Journal of Environmental Engineering*, 6 (132).
- 551 Butler, J.J. (1998). *The Design, Performance, and Analysis of Slug Tests*, New York: Lewis

552 Publishers.

553 Böer S. I., Arnosti, C., van Beusekom, J. E. E. and Boetius, A. (2009). Temporal variations in
554 microbial activities and carbon turnover in subtidal sandy sediments. *Bio- geosciences*, 6, 1149–
555 1165.

556 Carrier, W.D. 2003. Goodbye, Hazen; Hello, Kozeny-Carman. *Journal of Geotechnical and*
557 *Geoenvironmental Engineering*.1054.

558 Christodoulou & A. I. Stamou (eds). CRC Press, Taylor & Francis Group, Lon- don, ISBN 978-
559 0-415-58475-3.

560 de Marsily, G., (1986). *Quantitative Hydrogeology: Groundwater Hydrology for Engineers*,
561 Academic Press, N.Y.

562 Denham, M. and Vangelas, K. M. (2008). Biogeochemical gradients as a framework for un-
563 derstanding waste-site evolution. *Remediation*, 19 (1), 5-17.

564 Diaw, E. B., Lehmann, F., Ackerer, Ph. 2001. One-dimensional simulation of solute transfer in
565 saturated–unsaturated porous media using the discontinuous finite elements method. *Journal of*
566 *Contaminant Hydrology* 51(3-4): 197-213.

567 Environment Agency, (2001). The distribution of organotin compounds in water and sediments
568 in Liverpool Bay and the Mersey Estuary. *Environment Agency*, reMSP-01-07.

569 Fetter, C. W. (1999). *Contaminant Hydrogeology*. Second Edition, Prentice Hall Upper Saddle
570 River, NJ 07458.

571 Fischer, H. B., List, E. J., Koh, R. C. Y., Imberger, J., Norman, H. B., (1979). *Mixing in inland*
572 *coastal waters*. Academic Press, London.

573 Ford, D. and Williams, P. (1989). *Karst Geomorphology and Hydrology*, Unwin Hyman Ltd,
574 London.

575 Fox, W. M., Johnson, M. S., Jones, S. R., Leah, R. T., Copplestone, D. (1999). The use of
576 sediment cores from stable and developing salt marshes to reconstruct historical contamination
577 profiles in the Mersey Estuary, UK. *Marine Environmental Research*, 47, 311-329.

578 Freeze, R. A. and Cherry, J.A. (1979). *Groundwater*. Prentice-Hall, Inc., N. J.

579 Gray, D.M. and R.J. Granger (1986) In situ measurements of moisture and salt movement in
580 freezing soils. *Canadian Journal of Earth Science*, 23: 696–704.

581 Horn, D.P. (2002). Beach groundwater dynamics. *Geomorphology* 48, 121–146.

582 Huang, W.E., C.C. Smith, D.N. Lerner, S.F. Thornton, A. Oram. (2002). Physical modelling of
583 solute transport in porous media: evaluation of an imaging technique using UV ex- cited
584 fluorescent dye. *Water Research*, 36: 1843–1853.

585 Huettel, M., Ziebis, W. and Forster, S. (1996). Flow induced uptake of particulate matter in
586 permeable sea beds. *Limnology and Oceanography* 41: 309-322.

587 Itugha, O. D. (2008). Solute and particulate transport at the interface of near-shore permeable
588 estuarine beach-sand: an experimental study of the outer reaches of River Mersey estuary, N W
589 England. Harold Cohen; THESIS 20860.ITU, Liverpool: Thesis Ph.D., 2008

590 Itugha, O. D., Chen, D. and A.A. Ahmed (2010). Solute migration and transport in coastal sand-
591 beach sediments under strong tides. Vol. 2, 935-940. *In Environmental Hydraulics – G. C.*

592 Jones, P. D., (2006). Water quality and fisheries in the Mersey estuary, England: A historical
593 perspective. *Marine Pollution Bulletin* 53: 144–154.

594 Kalbus, E., Reinstorf, F., and Schirmer, M. (2006). Hydrology and Earth System Sciences, 10,
595 873–887, 2006

596 Khalili A, Basu AJ, Pietrzyk, U. (1998). Flow visualization in porous media via Positron
597 Emission Tomography. *Physics of Fluids*, 10:1031–3.

598 King, A.J., Readman J.W. and Zhou J.L. (2004). Determination of polycyclic aromatic hydro-
599 carbons in water by solid-phase microextraction - gas chromatography - mass spectrometry.
600 *Analytica Chimica Acta* 523(2): 259-267.

601 Klute, A., Dirksen, C. (1986). Hydraulic conductivity and diffusivity: laboratory methods. In:
602 Klute, A. (Ed.), *Methods of Soil Analysis. Part 1. Physical and Mineralogical Methods*, 2nd ed.
603 Agron. Monogr. 9. ASA, Madison, WI, pp. 687–734.

604 Lanyon, J. A., Eliot, I. G. Clarke, D. J. (1982). Groundwater–level variation during semidiurnal
605 spring tidal cycles on a sandy beach. *Aust. J. Mar. Freshwater Res.* 33: 377-400.

606 Li, H., Sun, P. Chen, S., Xia, Y. and Liu, S. (2009). A Falling-Head Method for Measuring
607 Intertidal Sediment Hydraulic Conductivity. *Ground Water*, doi: 10.1111/j.1745-
608 6584.2009.00638.x

609 Li, L., Barry, D.A., Pattiaratchi, C.B. (1997). Numerical modelling of tide-induced beach water
610 table fluctuations. *Coastal Engineering* 30, 105–123.

611 Li, Y., Ghodrati, M. (1995). Transport of nitrates in soils as affected by earthworm activities.
612 *Journal Environmental Quality* 24: 432-438.

613 Mao, X., Enot, P., Barry, D.A., Li, L., Binley, A., Jeng, D.-S. (2006) Tidal influence on be-
614 haviour of a coastal aquifer adjacent to a low-relief estuary. *Journal of Hydrology*, 110–127.

615 McNeil, J. D., Oldenborger, G. A., and Schincariol, R. A. (2006). Quantitative imaging of
616 contaminant distributions in heterogeneous porous media laboratory experiments. *Journal of*
617 *Contaminant Hydrology* 84: 36–54.

618 Nakano, Y. (1995). *Transport of Tracer Br in Frozen Morin Clay in Response to Temperature*
619 *Gradients*. Cold Regions Research & Engineering Laboratory (CRREL) Report 95-3. US Army
620 Corps of Engineers.

621 Nielsen, P. (1999). Groundwater Dynamics and Salinity in Coastal Barriers. *Journal of Coastal*
622 *Research*, 15(3), 732-740.

623 Nielsen, P., 1990. Tidal dynamics of the water table in beaches. *Water Resources Research* 26:
624 2127-2134.

625 Peck, L. (1998). *Remediation of Wastewater by Land Treatment Consideration of Soil*
626 *Temperatures in Winter*. Cold Regions Research & Engineering Laboratory (CRREL) Report
627 98-8. US Army Corps of Engineers.

628 Philip, J. R. 1973. Periodic non-linear diffusion: an integral relation and its physical conse-
629 quences. *Australian Journal of Physics* 26: 513–519.

630 Precht, E., Huettel, M. (2004). Rapid wave-driven advective pore water exchange in a permeable
631 coastal sediment. *Journal of Sea Research*, Vol. 51, pp. 93–107.

632 Reimers, C. E., Stecher III, H. A., Taghon, G. L., Fuller, C. M., Huettel, M., Rusch, A.,
633 Ryckelynck, N., Wild, C. 2004. In situ measurements of advective solute transport in permeable
634 shelf sands. *Continental Shelf Research* 24 (2004) 183–201.

635 Robbins, G. A. 1989. Methods for determining transverse dispersion coefficients of porous-
636 media in laboratory column experiments. *Water Resource Research* 25:1249–1258.

637 Rogers, H. R. (2002). Assessment of PAH contamination in estuarine sediments using the
638 equilibrium partitioning–toxic unit approach. *Science of the Total Environment* 290:139–55.

639 Schincariol, R.A., Herderick, E.E., Schwartz, F.W. (1993). On the application of image analy-
640 sis to determine concentration distributions in lab expts. *J. of Contaminant Hydrol.* 12: 197-215.

641 Schirmer, M., Molson, J.W., Frind, E.O., Barker, J.F. (2000). Biodegradation modelling of a
642 dissolved gasoline plume applying independent laboratory and field parameters. *Journal*
643 *Contaminant Hydrology*, 46 (3–4), 339–374.

644 Shum, K. T. and Sundby, B. (1996) Organic matter processing in continental shelf sediments -
645 the subtidal pump revisited. *Marine Chemistry*. 53:81-87.

646 Sundby, B. (2001). Permeable marine sediments: Overturning an old paradigm. *EOS Transcripts*
647 *Am. Geophysics*, 82, 135-136.

648 Swartz, C. H. and Schwartz, F. W. (1998): An experimental study of mixing and instability
649 development in variable-density systems, *Journal of Contaminant Hydrology* 34: 169–189.

650 Todd, D. K. (1980). *Groundwater hydrology*, 2nd edition. Wiley, New York.

651 Turner, I. L., and Nielsen, P., (1997). Rapid Water Table Fluctuations within the Beach Face :
652 Implications for Swash Zone Sediment Mobility. *Coastal Engineering* , 37, 45-59.

653 Turner, I. L., Coates, B. P. and Acworth, R. I. (1996). The Effects of Tides and Waves on Water-
654 Table Elevations In Coastal Zones. *Hydrogeology Journal* 4(2): 51-69.

655 Vane, C.H. I. Harrison, A.W. Kim (2007). Polycyclic aromatic hydrocarbons (PAHs) and
656 polychlorinated biphenyls (PCBs) in sediments from the Mersey Estuary, U.K. *Science of the*
657 *Total Environment*, 374, 112–126.

658 Webster, I. T., and Taylor, J. H., (1992). Rotational dispersion in porous media due to
659 fluctuating flows. *Water Resources Research* 28: 109-119.

660 Weight, W. D., Sonderegger, J. L. (2001). *Manual of Applied Field Hydrogeology*. McGraw-
661 Hill Companies, Inc., USA.

662 Wexler, E. J. (1992). *Analytical solutions for one-, two-, and three dimensional solute transport*
663 *in groundwater systems with uniform flow*. USGS-TWRI Book 3, Chap B7.

664 Wilson, A. M. and Gardner, L. R. (2006). Tidally driven groundwater flow and solute exchange
665 in a marsh: Numerical simulations. *Water Resources Research*, Vol. 42, W01405.

666 Woodworth, P.L., Tsimplis, M.N., Flather, R.A., Shennan, I., (1999). A review of the trends
667 observed in British Isles mean sea level data measured by tide gauges. *Geophysical Journal*
668 *International* 136 (3), 651-670.

669 Woodworth, P. L. and Blackman, D. L. (2002). Changes in Extreme High Waters At Liverpool
670 Since 1768. *International Journal of Climatology* 22: 697–714 (2002).

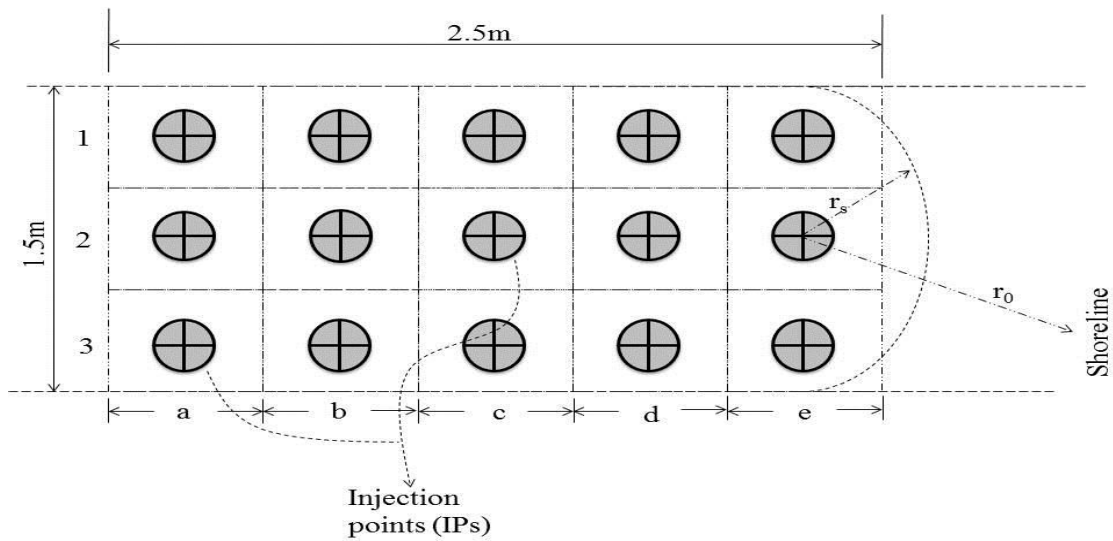
671 WPRL (1974). Effect of Polluting Discharges on the Mersey Estuary. Report of Investigations
672 on behalf of the Steering Committee on Pollution of the Mersey Estuary. WPRL Report 447R.

673 Zhang, Q.; Volker, R. E.; Lockington, D. A. (2002). Experimental investigation of contaminant
674 transport in coastal groundwater. *Advances in Environ. Res.* 6: 229-237.

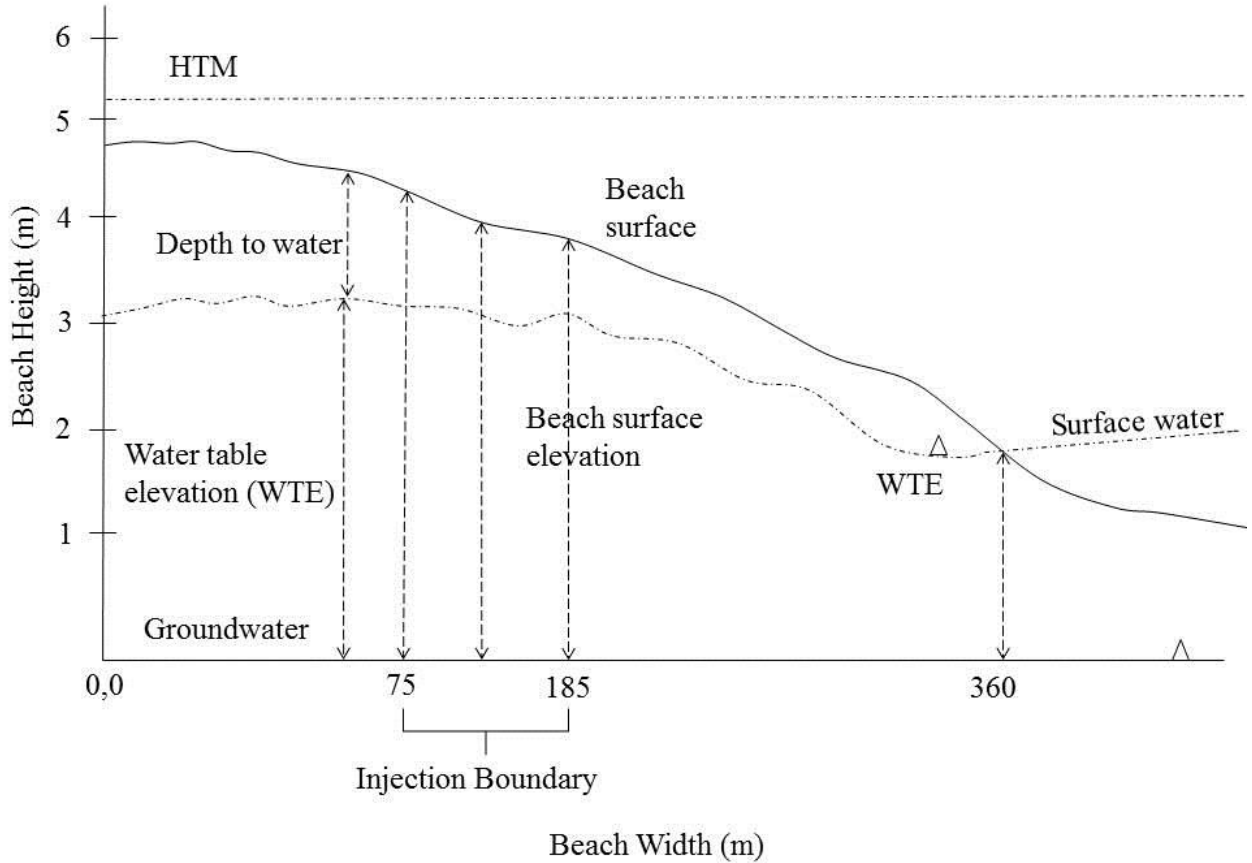
675
676



677
678 Fig 1: Area map with markers showing the injection zones and Marine Lake at the sheltered
679 boundary of the outer RME with overview map (*at the right shows the RME*).



680
681 **Fig 2:** Arrangement of rectangular cross-section of IPs in a typical field site with column/row
682 divisions (*columns are represented by a, b, c, ..., and rows by 1, 2 & 3 such that a₁, a₂, ... represent IPs in the 1st*
683 *column, etc.; r_s = radial distance at a point from an IP; r₀ = radius of influence, a function of the shoreline distance*
684 *and permeability.*)



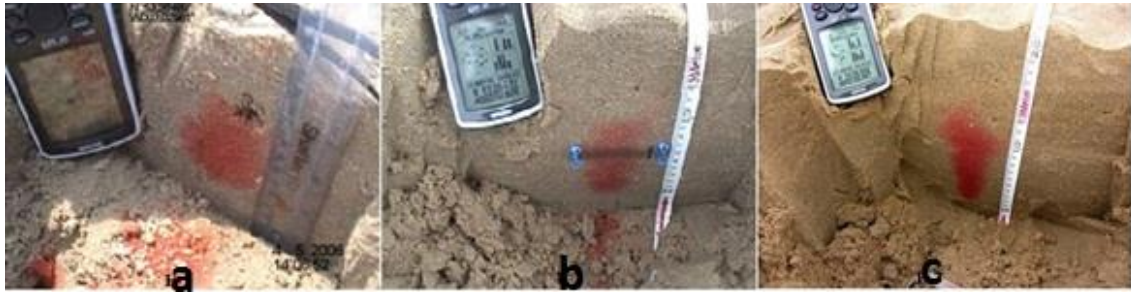
685 Fig 3: Sketch illustrating the intertidal (shoreline - inland bank) divisions with water table elevation
 686 (WTE), injection area and tidal water marks at the RME [*high tide mark (HTM)*]
 687

688 Table 1: Summary of field experiment during the summer (April-July 2006; 2007)

Experimental Area	Injection Zone	Number of IP locations @		Total IPs @		Total IPs mined @	
		3*5 array	5*5 array	3*5 array	5*5 array	3*5 array	5*5 array
N56 26 W03 02	OEIS-IZ (A)	57	4	855	100	513	65
N56 26 W03 03	OEIS-IZ (B)	32	2	480	50	264	30
	OEIS-IZ (C)	7	1	105	25	63	10
N56 26 W03 02	NEIS-IZ (A)	16	2	240	50	99	35
	NEIS-IZ (B)	6	1	90	25	27	10
Total				1770	250	966	150

689
 690
 691
 692
 693
 694
 695
 696
 697
 698
 699

700



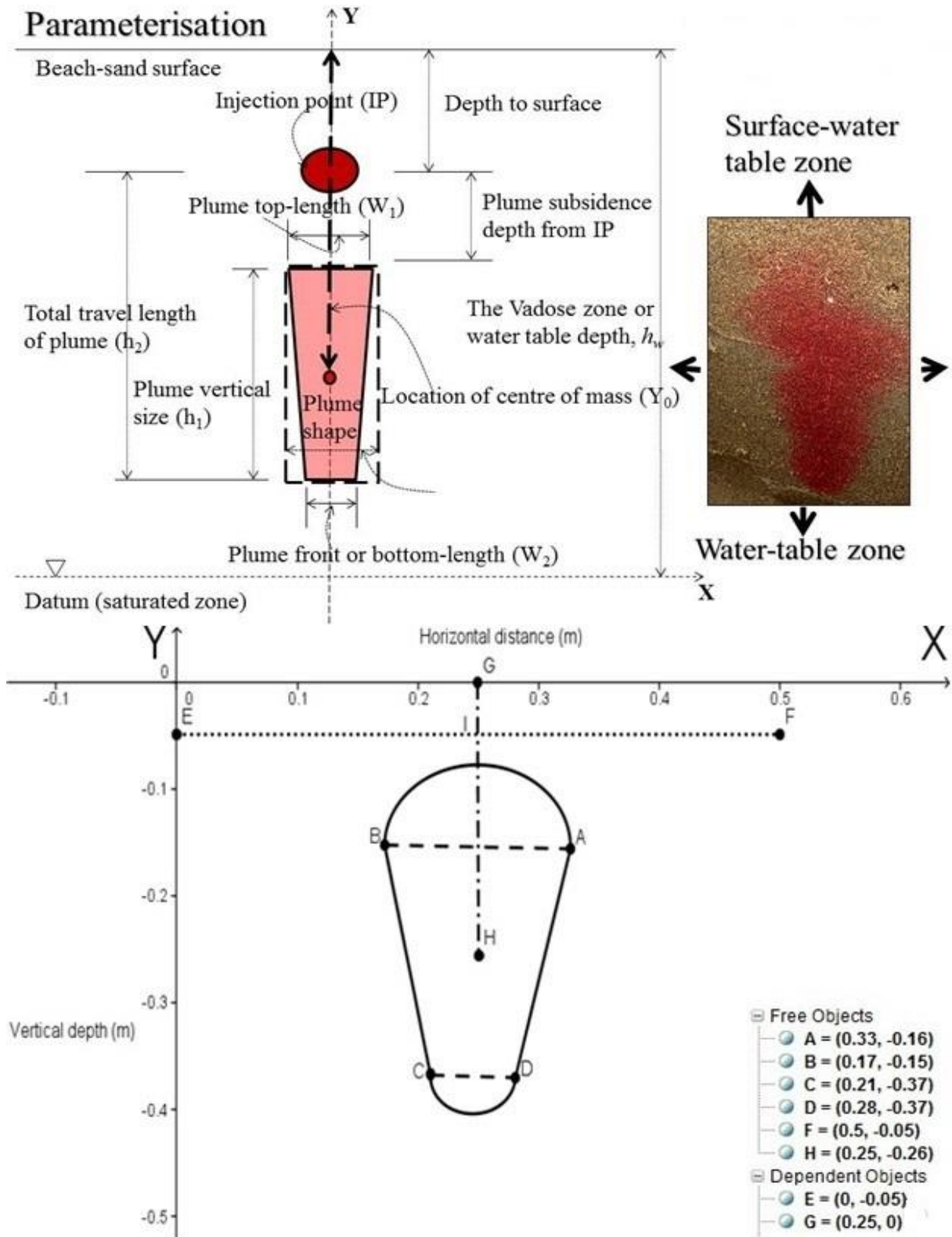
701

702

703

704

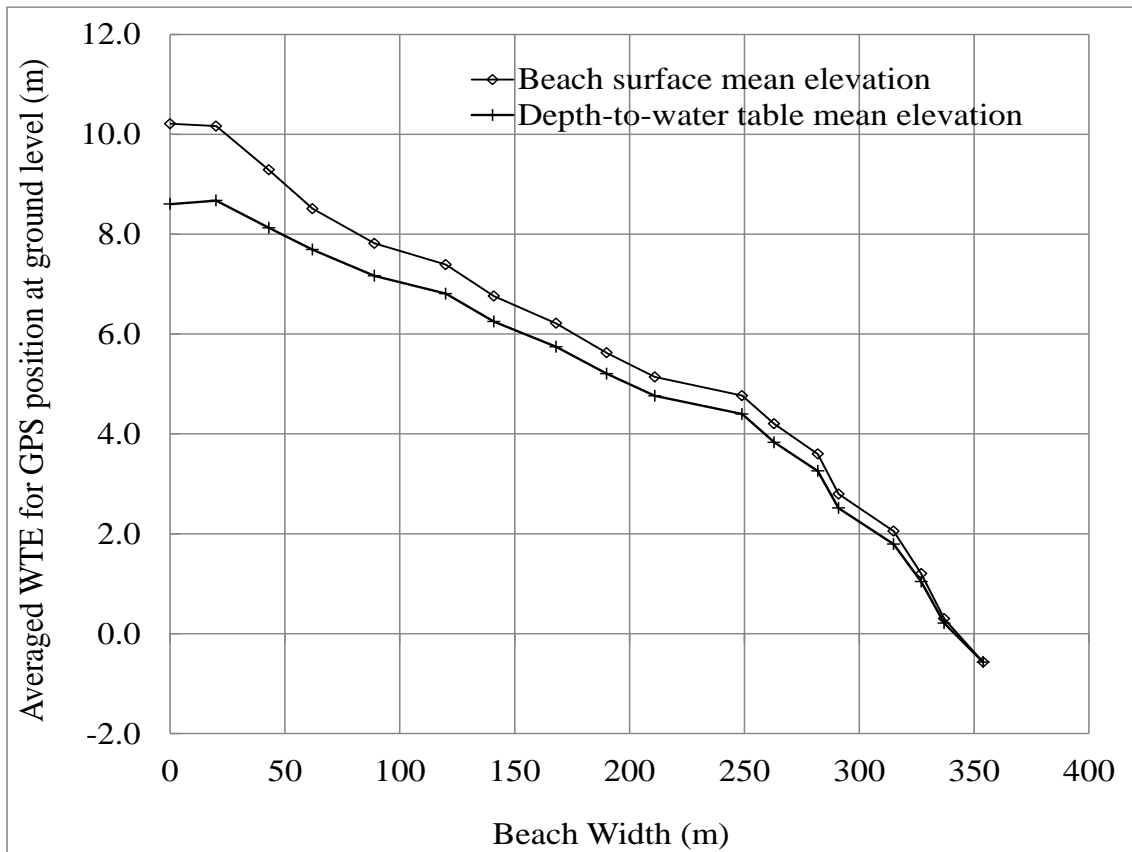
Fig 4: (a) about 4-5 hours after injection (no flood case), (b) after one complete tidal cycle and (c) two complete tidal cycles.



705

706 Fig 5: The upper part illustrates the parameter of the plume and direction of movement in space
 707 and the lower graph shows analysis of the plume with coordinates using a trapezoidal identity.

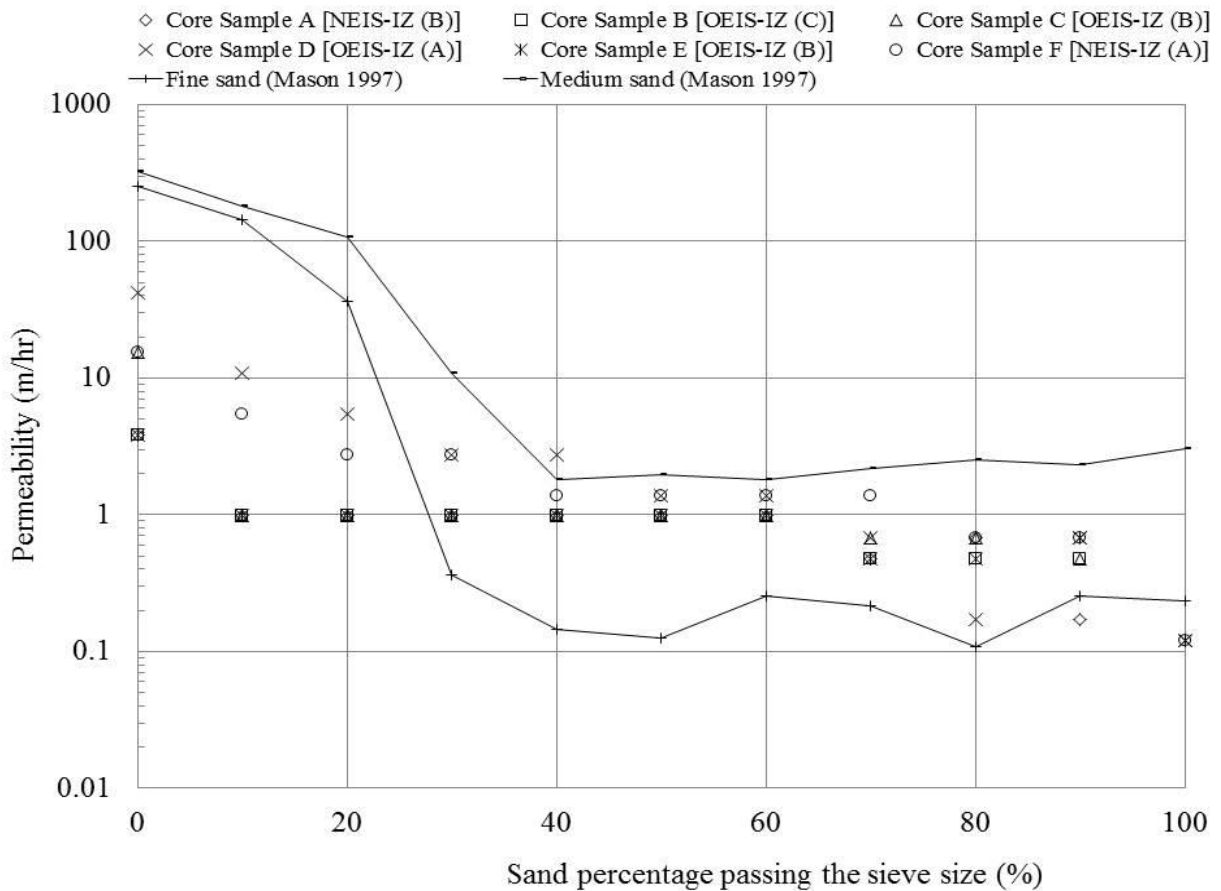
708 [$BA = W_1$, $CD = W_2$, $EF = 0.5\text{m}$ length of square cell, $GI = \text{depth to surface}$, $GH = \text{location of centre of mass}$]



709

710

Fig 6: Water table elevation relative to the beach surface elevation at the OEIS-IZ (A)

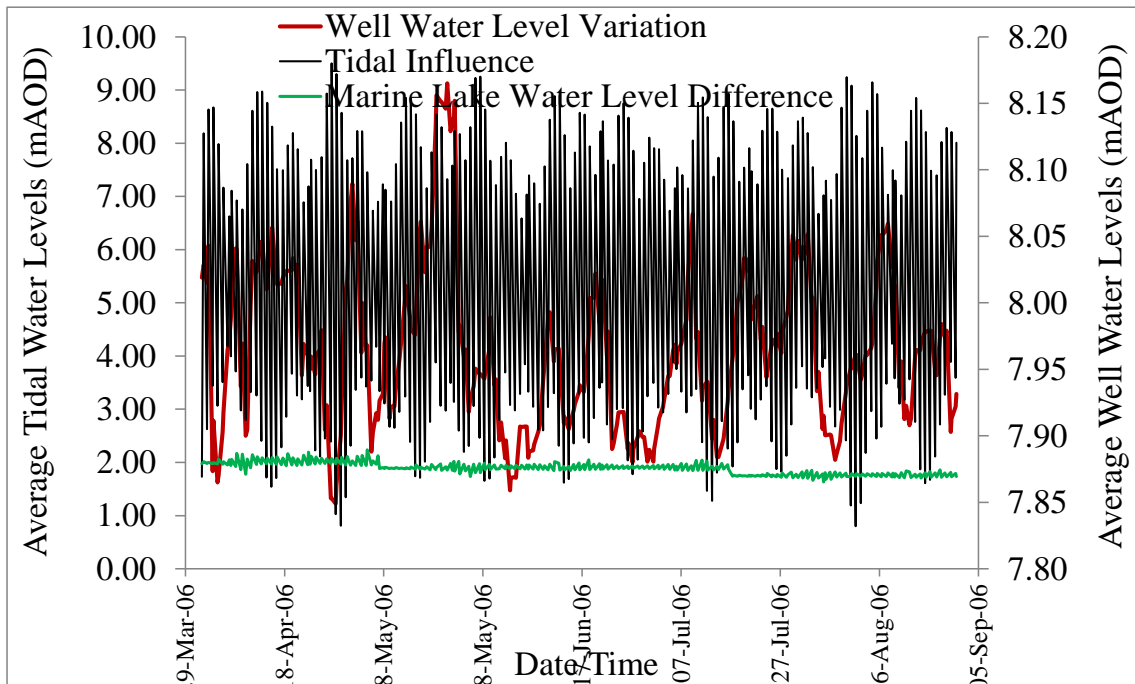


711

712

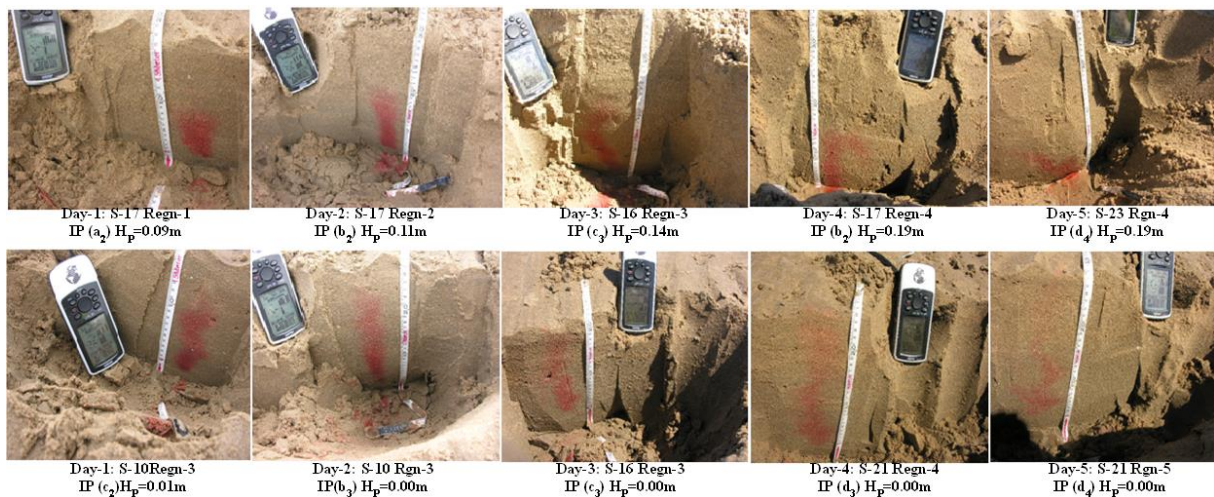
713

Fig 7: Permeability of core samples taken from injection sites showing grain-size differences using the Kozeny-Carman relation.



714
715

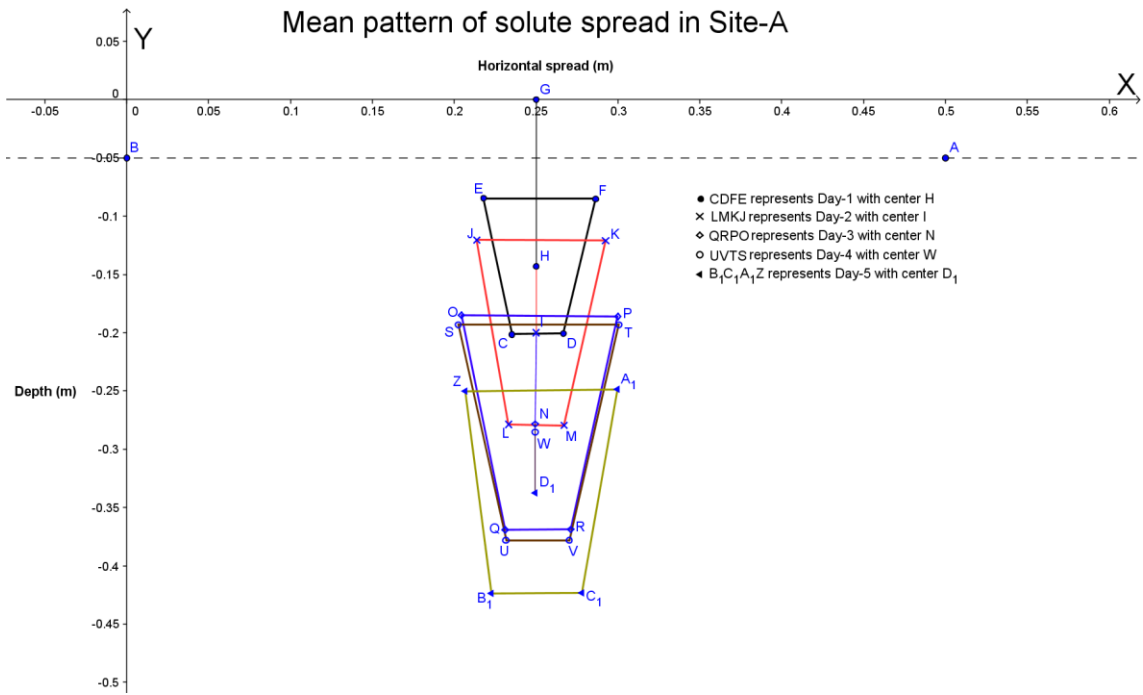
Fig 8: Correlation of SWL and groundwater level changes at the sheltered coast



716

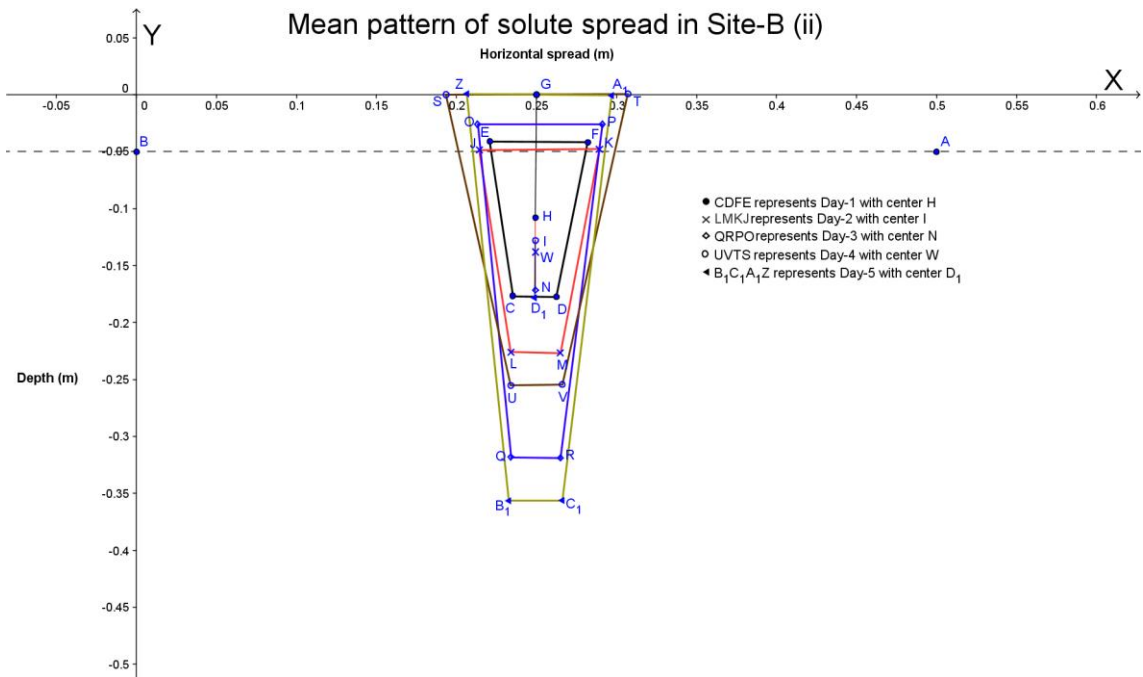
717 Fig 9: Plume subsidence from high conductivity (permeability) into low conductivity depth as
 718 observed in-situ at OEIS-IZ(A) – Top; Plume spread in low & high conductivity zones as observed
 719 in-situ at OEIS-IZ (B) – Bottom. [site (S), Regn (region), IP (injection point), 5ml/5cm (solute
 720 amount injected is 5ml and injection depth is 5cm), H_p (height of plume-top below injection-depth)]

721



722

723 Fig 10: Averaged features of conical plume at Site-A [OEIS-IZ (A)] for day 1; day 2; day 3; day
724 4; day 5

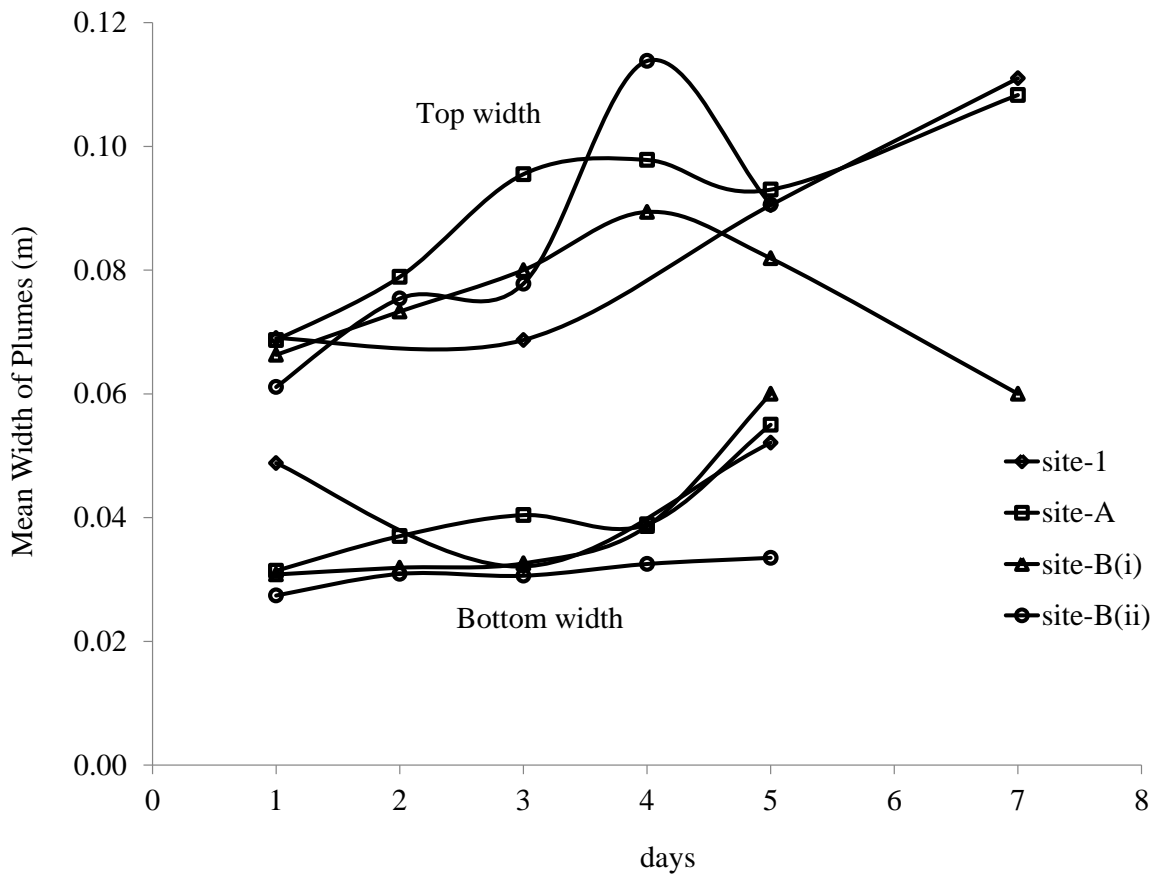


725

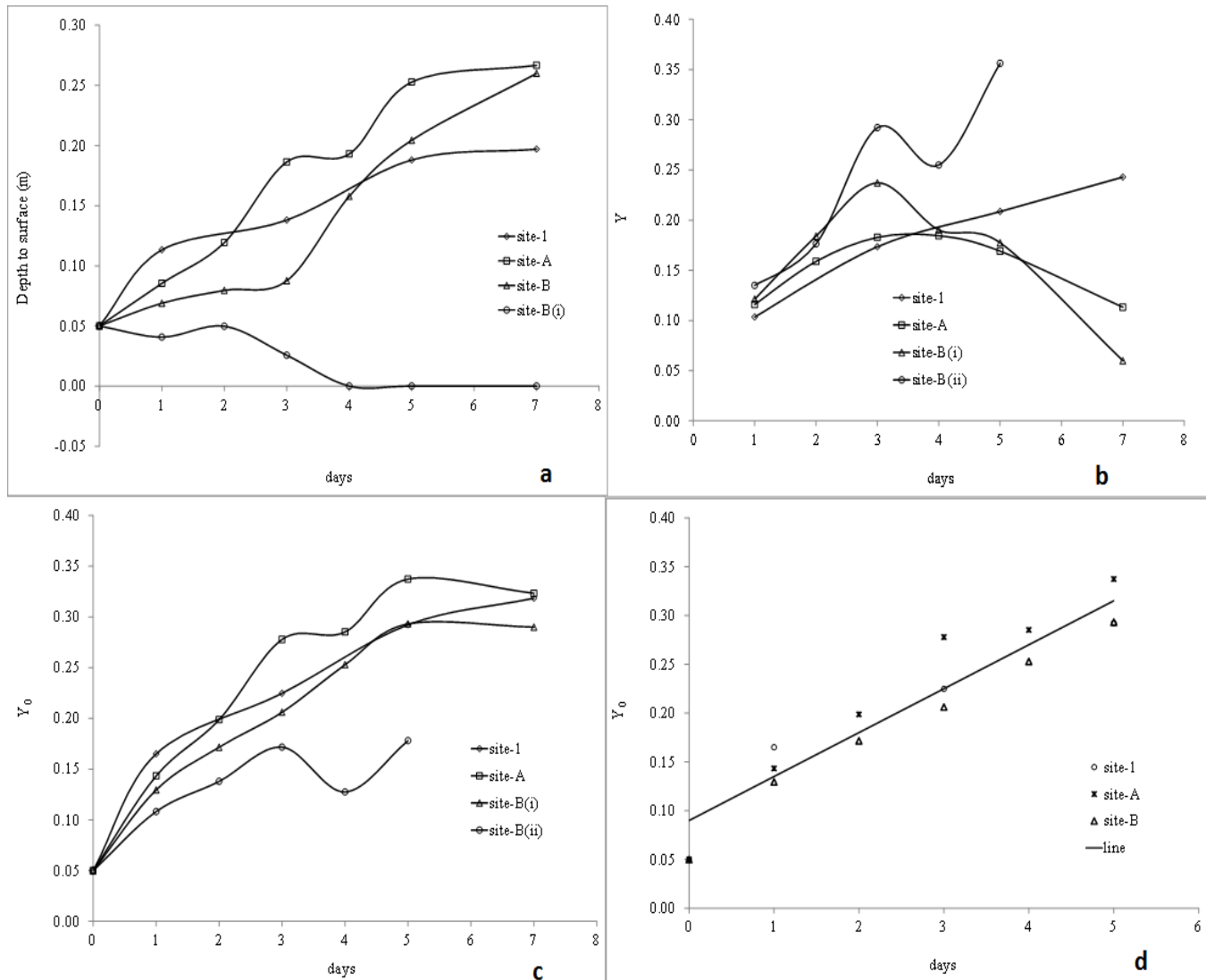
726 Fig 11: Averaged features of conical plume yield with depth in Sites B(ii) [OEIS-IZ (B)] for day
727 1; day 2; day 3; day 4; day 5

728

729



730
 731 Fig 12: Comparisons of the variations of mean top widths and bottom widths of plumes in Sites (1,
 732 A & B)
 733
 734
 735



736
737
738
739

Fig 13: Comparisons in Sites 1, A & B: (a) Mean variation of plumes in space away from the beach-sand surface with time. (b) Mean vertical length of plumes. (c) Mean depth of plume center of mass to surface. (d) Linear model with regression line for deepening center of mass.